PHYSICAL REVIEW LETTERS

Observation of Hybrid Soliton Vortex-Ring Structures in Bose-Einstein Condensates

Naomi S. Ginsberg,[1,*] Joachim Brand,[2] and Lene Vestergaard Hau[1]

[1]*Department of Physics and Division of Engineering and Applied Sciences, Harvard University,
Cambridge, Massachusetts 02138, USA*
[2]*Max Planck Institute for the Physics of Complex Systems, 01187 Dresden, Germany*

We present the experimental discovery of compound structures comprising solitons and vortex rings in Bose-Einstein condensates. We examine both their creation via soliton-vortex collisions and their subsequent development, which is largely governed by the dynamics of interacting vortex rings. A theoretical model in three-dimensional cylindrical symmetry is also presented.

Quantized vortices have long been considered a signature of superfluidity in helium II [1]. The recent emergence of Bose-condensed alkali gases provides a new and different arena for studying quantum fluids, their excitations, and interactions of the latter. In addition to observing vortices alone [2–4], experimentalists have reported observations of gray solitons [5,6] and their decay into vortex rings (VRs) [7,8] via the Kadomtsev-Petviashvili, or "snake," instability [9].

In this Letter, we present the observation of a new class of topological excitations in Bose-Einstein condensates (BECs): hybrid structures originating from a combination of gray solitons and VRs. By "gray soliton," we mean a nondispersive, nonlinear solitary wave whose phase profile and velocity are determined by its variably depleted amplitude. In contrast with the conventional 1D soliton, solitary waves in higher dimensions, such as those observed in this work, may decay and also interact with other nonlinear excitations in a nontrivial fashion. Thus the solitonic wave fronts we describe extend on 2D sheets, whereas vortex structures have a depleted core and phase singularity along a 1D filament, which may loop to form a VR. We detail how these nonlinear excitations initially collide and how the subsequent compound structure dynamics diverge from those of the superposed evolution of individual excitations. To date, the interplay between solitons and vortices has been explored only theoretically [10–12].

In previous work [8], we studied gray solitons and vortices generated from the quantum analog of shock waves by creating a single, narrow density defect in a BEC. We presently optimize the likelihood of collisions between these excitations by creating two symmetrically placed defects via a mechanism similar to that used in [8].

A thin wire blocks the "coupling" beam from illuminating the center of a magnetically trapped BEC [Fig. 1(a)], to create a symmetric *double light-roadblock*. We then inject two counterpropagating Gaussian-shaped "probe" pulses along the symmetry axis of the trap. The pulses compress spatially by several orders of magnitude via the slow-light technique [13] and ultimately fit entirely inside the BEC. The probe beams are resonant with the

atoms' internal $|1\rangle$–$|3\rangle$ transition while the coupling beam is resonant with the $|2\rangle$–$|3\rangle$ transition [Fig. 1(b)].

When the pulses arrive at the wire's shadow, their propagation is effectively arrested and they are further compressed [8]. Atoms at the halted pulses' locations are then ejected, having first been transferred from initial state, $|1\rangle$, to $|2\rangle$ (untrapped) via a slow-light induced dark state. This results in two deep, narrow density defects in $|1\rangle$, symmetric about the BEC's center [Fig. 1(c)].

For the current experiment, we condense 3.6×10^6 sodium atoms in $|1\rangle$ and employ trap frequencies $\omega_z = 2\pi \times 21$ Hz and $\omega_x = \omega_y = 3.0\omega_z$ in our 4-Dee magnetic trap [14]. We work at temperatures well below the transition temperature to BEC so there is virtually no noncondensed component. The coupling (peak probe) Rabi frequency is $2\pi \times 15.3$ (3.8) MHz, and duration (probe $1/e$ half-width) is 12 (2.5) μs. We use a 35 μm wire mask.

After creating the defects, we vary the duration of condensate evolution in the magnetic trap, Δt_{trap}, and then release the condensate and let it expand for $\Delta t_{\text{exp}} = 19.9$ ms before using a slice technique [8,15] to image
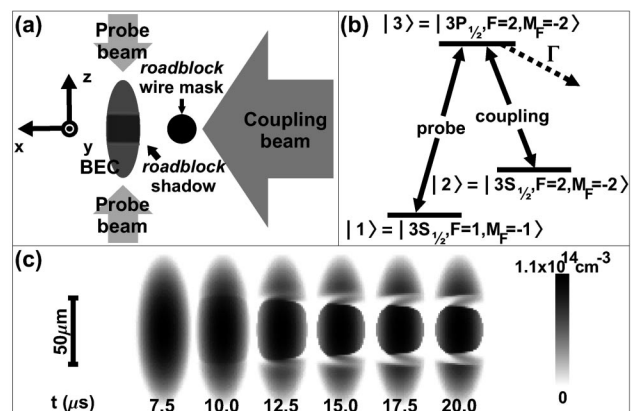

FIG. 1. Defect creation. (a) Double light-roadblock setup. (b) Energy level diagram. (c) Density plots of $|1\rangle$ atoms from 2D simulations of defect creation using a 60 μm wire mask; initially, the BEC has 4.0×10^6 atoms. Light pulse intensities and durations are as in the experiment.

the central 20–30 μm thick slab of the expanded cloud in the x-z plane. Figure 2(a) shows the "control" experiment in which a single probe pulse is injected into the BEC, while Fig. 2(b) depicts the double-roadblock experiment in which interactions between excitations are evident.

The early dynamics that ensue from the creation of a single defect are detailed in Fig. 3 of [8]. The defect splits into two density dips propagating at the sound speed in the $+z$ and $-z$ directions, while the back edge of each steepens due to the density dependence of the sound speed. In a classical fluid, this would lead to shock wave formation; i.e., the back edges would develop infinite slope. In a superfluid, significant density changes over distances shorter than the healing length cannot occur [16]. Consequently, as the density dips travel, they shed gray solitons each time their back edges become too steep [8]. As observed in Fig. 2(a), the solitons, although stable in 1D, kink and decay into vortex structures via the snake instability, seeded predominantly by the transverse density variation of the condensate depicted in Fig. 1(c).

We now describe the experimental data in Fig. 2, comparing and contrasting the transmission images of the double-defect experiment with the control experiment, before considering a corresponding theoretical simulation. Focusing mostly on structures between the two initial defects, we see at $\Delta t_{\text{trap}} = 0.1$ ms in Fig. 2(b) that solitons (pale stripes) have already shed from density dips originally emanating from the defects. High-density (dark) bands on the top and bottom result from the rush of fluid into the defect locations. The first solitons shed are the deepest, hence slowest moving, and therefore bound the regions of high density. In the center, between these first solitons, secondly shed ones have kinked so that they overlap on the sides but not in the middle, forming a checkerboard pattern. This is clearly seen at $\Delta t_{\text{trap}} = 0.4$ ms where the images also show VR cores in the

"four corners." Figure 2(b) at 0.1 and 0.4 ms and Fig. 2(a) at 0.5 ms are comparable. The single-defect image shows additional shallower solitons in the wake of the traveling density dip, which are initially hidden in the double-defect version by the mirror image of higher-contrast structures. At $\Delta t_{\text{trap}} = 1.1$ ms [Fig. 2(b)], the soliton curvature has increased further. As at 1.3 ms of Fig. 2(a), the deepest solitons form double-cusped shapes ["W" ("M") on top (bottom)] that span the cloud from side to side. The second pair of solitons propagates toward one another further, closing off a region of fluid in the center.

We have explored the 3D structure of the excitations by varying the y position of the imaged slice to find that the system is highly cylindrically symmetric. Thus, the white loop in the center at 1.1 ms and the pairs of flattened loops at $\Delta t_{\text{trap}} = 1.3$ and 1.7 ms represent roughly ellipsoidal *shells* of low density, a feature clearly absent in the single-defect case. Comparing the latter two time points with $\Delta t_{\text{trap}} = 2.1$ ms in Fig. 2(a), we conclude that the centers of the deepest solitons have decayed into VRs, forming the equatorial components of their corresponding closed low density shells in Fig. 2(b). The upper and lower "hemispheres" of the shells all derive from solitons formed after the first (deepest) ones that produced VRs.

At $\Delta t_{\text{trap}} = 2.3$ ms in Fig. 2(b), the closed structures appear to interlace and subsequently form a single low density shell at the center of the condensate (2.8–6.0 ms). This provides very strong evidence that the double-defect dynamics are not merely a superposition of mirrored single-defect dynamics. At $\Delta t_{\text{trap}} = 4.1$ ms, Fig. 2(a) displays a soliton fragment in the center with a VR below. At 4.4 ms in Fig. 2(b), the low density structure is *closed* and could not be formed from the superposition of elements from the corresponding time point in Fig. 2(a).
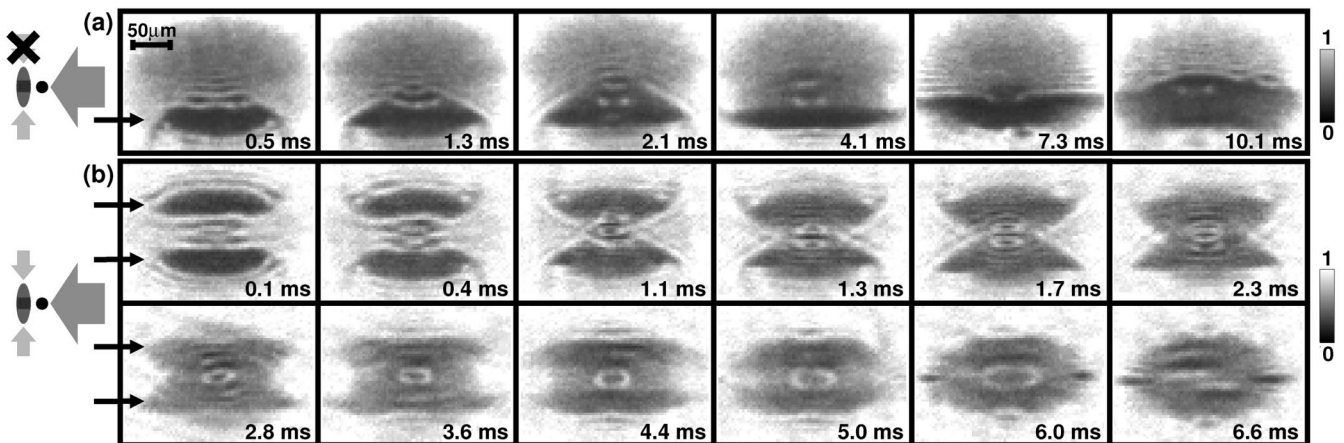

FIG. 2. Experimentally observed resonant transmission images of BECs (transmitted laser intensity normalized to incident) after they are illuminated with coupling and probe pulse(s). In (a) [(b)], one [two] probe pulse[s] is [are] hitting the cloud, there are initially $4.0\,[3.6] \times 10^6$ condensed atoms, and the imaged slice is 30 [23] μm thick. Times cited refer to evolution time in the trap, Δt_{trap}, after defect creation; $\Delta t_{\text{exp}} = 19.9$ ms. The arrows indicate initial defect planes.

This single-shell compound structure maintains its shape for over 4.0 ms. At 6.6 ms, we observe that what was a closed shell has sheared and come apart at the sides. The resulting structures break cylindrical symmetry, highlighting their sensitivity to torque from the laser beams, evident in Fig. 1(c). Furthering the case for interactions rather than superposition, the last two frames of Fig. 2(a) have a long-lived VR in the center, in stark contrast with Fig. 2(b) at 6.6 ms, which has segments that could not be constructed from VRs alone.

We measure the soliton and shell half-widths to range from 3 to 6 μm, comparable to a calculated healing length of 4 μm [17]. We also note the collective modes in the BEC produced by the initial rush of fluid into the defects' locations. The high-density bands in both Figs. 2(a) and 2(b) breathe and bend. We find these modes are highly dependent on the initial defect shape.

To complement our observations, we have performed simulations based upon a generalized Gross-Pitaevskii (GP) description [18] for three phases of BEC evolution as follows: We first simulate defect creation via slow-light propagation on a 2D spatial grid, as in Fig. 1(c). The atoms in $|2\rangle$ are quickly ejected from the trap and we map a symmetrized version of the resulting defect in the $|1\rangle$ condensate onto a 3D cylindrically symmetric grid. We then calculate in-trap evolution of the $|1\rangle$ atoms for a duration Δt_{trap} and finally continue to follow the BEC evolution after the trapping potential is turned off.

The results of simulations for $\Delta t_{\text{exp}} = 14$ ms with varying Δt_{trap} are shown in Fig. 3. (After 14 ms of cloud expansion, all topological dynamics are frozen out and further evolution simply leads to spatial magnification of the developed features; the BEC's aspect ratio differs from that at 19.9 ms by $\sim 15\%$.) We see the same prominent features in the simulation as in the experiment, allowing us to identify the nature of the low density shells. Phase information confirms the existence of solitons and identi-
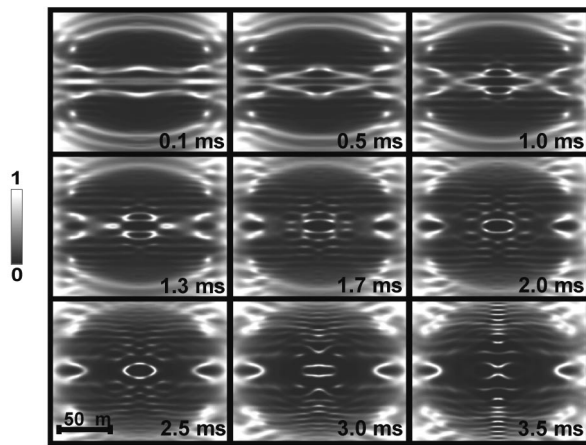

FIG. 3. Simulation for $\Delta t_{\text{exp}} = 14$ ms (Δt_{trap} on plots) with parameters as in Fig. 1(c). To compare with experiment, we plot the transmission, $e^{-D_y(x,z)}$, where $D_y(x,z)$ is the optical density along y over the central 22 μm slab of the BEC.

fies the creation and annihilation of VRs. Experimental parameters have been chosen within a regime in which VRs are produced but parent solitons are not destroyed. (Our simulations suggest that this phenomenon occurs for densities between 6×10^{12} cm^{-3} and 4×10^{13} cm^{-3}.)

The simulation follows the experiment up to $\Delta t_{\text{trap}} \sim 1.3$ ms, after which point evolution is slightly accelerated. Other discrepancies include reduced soliton curvature and less dramatic collective mode breathing than in the experiment. This could be a result of the different initial defect separation used in the theory to generate a sequence most comparable to the data.

Despite these differences, the simulations provide us with the history of the experimentally observed structures that must be expanded to be optically resolved. Calculations show that if two solitons are incident on one another, the time taken for them to reach each other and their degree of kinking as they meet have different density dependencies. During expansion but before interaction energy is completely converted to kinetic, soliton translational velocity and the rate of soliton kinking both decrease as BEC density drops, but at different rates. This implies that expansion evolution is important for generating the observed defect collision dynamics and is different than in-trap evolution. Consequently, expansion sequences following different Δt_{trap} are not mere duplicates offset from one another in time. A typical variation in such sequences is the occurrence of VR creation and annihilation at slightly different points in the evolution.

As an example, we present the simulated release dynamics for $\Delta t_{\text{trap}} = 3.0$ ms in Fig. 4. As in the experiment, the first soliton (blue) shed from each of the waves traveling toward the BEC's center is the deepest, slowest, and least stable, leading to decay into VRs at $\Delta t_{\text{exp}} = 1.5$ ms. Solitons created after the first ones (green through red, in order of creation from the top defect) propagate across the center line of the BEC ($\Delta t_{\text{exp}} = 1.5$ and 3.0 ms); those with opposite propagation directions sometimes overlap. As the third and fourth generated solitons reach the newly formed VRs on the side opposite whence they originated, we observe pairs of low density shells ($\Delta t_{\text{exp}} = 4.0$ ms). By examining the phase, we confirm, as discussed for images 1.3 and 1.7 ms of Fig. 2(b), that these shells are made from VRs and transiently passing soliton fronts.

The second deepest (secondly shed, green) solitons cross in the center of the BEC as their midpoints bend toward one another (also $\Delta t_{\text{exp}} = 4.0$ ms). As these fronts reach the VRs at 5.0 ms (again forming a pair of low density shells), the central portions of the solitons curve further, producing within themselves two smaller VRs with opposite circulation from the larger ones. Thus, both above and below the central horizontal plane, the two concentric VRs are embedded in a roughly hemispherical solitonic shell, forming a hybrid structure that will "dislocate" from the remaining outer edges of the soliton front. The smaller VRs are evident from the wave function's phase even
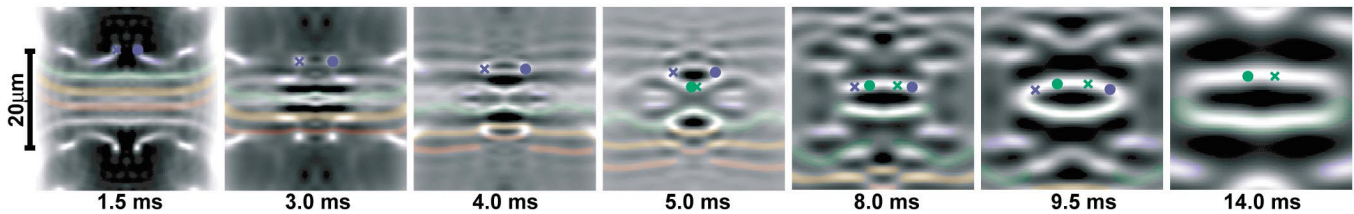
FIG. 4 (color).   Simulation of soliton VR dynamics during expansion after $\Delta t_{\mathrm{trap}} = 3.0$ ms. Times cited are Δt_{exp}. Only solitons propagating in the $-z$ direction (downward) from the $+z$ (top) defect are shaded (blue through red, in order of creation), to assist in tracking the movement of each from frame to frame. Dots (crosses) indicate vortex cores for $z > 0$ *only* with positive (negative) circulation with respect to the plane of the page. The vortex colors correspond to parent soliton colors, although the green cores are generated by the mirror image of the correspondingly shaded soliton. Density ranges from 0 to $\{7.5, 4.5, 4.1, 3.6, 1.3, 0.92, 0.42\} \times 10^{13}$ cm^{-3} for each of the times presented, respectively. Simulation parameters are the same as in Fig. 1(c).

though they are not distinguishable in the density plots. The general motion of the hybrid segments is largely determined by the velocity fields from the vortices present. Like an umbrella turning inside out, the curvature of these hybrid structures reverses through $\Delta t_{\mathrm{exp}} = 8.0$ ms, as the inner rings propel themselves away from one another and the outer rings propel toward the center line. This occurs in the experiment for $\Delta t_{\mathrm{trap}} = 2.3$ ms and in Fig. 3 at 1.7 ms. The VRs behave as the "phantom" propellers in the compound structures.

As the outer VRs propagate toward each other, a closed shell forms from the two hybrid segments ($\Delta t_{\mathrm{exp}} = 9.5$ ms). It is an ellipsoidal solitonic shell incorporating four VRs of alternating circulation that encircle the structure like lines of constant latitude on a globe. The outer VRs eventually annihilate (quantized circulation at the VR cores disappears). Subsequently, the two segments that formed the central shell lose their curvature, and the shell breaks up along $z = 0$. This is seen at $\Delta t_{\mathrm{exp}} = 14$ ms (a close-up of the BEC at $\Delta t_{\mathrm{trap}} = 3.0$ ms in Fig. 3) and should be compared to the experimentally observed shearing at 6.6 ms in Fig. 2(b).

In light of these observations it is natural to ask whether low density shells can exist as stationary states in a BEC. We have shown that the GP equation exhibits stationary solutions in spherical symmetry consisting of an inner sphere of almost constant density surrounded by low density shells similar to Bessel-function-type spherical waves, $\sin(kr)/r$. This has been independently treated by others [19]. In a trap, solutions with a finite number of particles and shells are possible; details will be given elsewhere. Unlike the observed structures discussed above, the stationary states show no vortex core formations. However, the observed hybrid shells might play a role in the decay of the stationary solutions.

In brief, we have presented the experimental observation and theoretical confirmation of low density shells in a fully 3D BEC, consisting of complex hybrid soliton-vortex-ring structures. VR propulsion, attraction, and annihilation heavily influence the structures' dynamics. The BEC's decreasing density, after a confining trap is switched off, contributes critically to the dynamics, as the resulting

regime is on the cusp of stability of solitons typically subject to the snake instability in 3D.

*Electronic address: ginsber@fas.harvard.edu

[1] R. J. Donnelly, *Quantized Vortices in Helium II* (Cambridge University Press, Cambridge, U.K., 1991).
[2] M. R. Matthews *et al.*, Phys. Rev. Lett. **83**, 2498 (1999).
[3] K. W. Madison, F. Chevy, W. Wohlleben, and J. Dalibard, Phys. Rev. Lett. **84**, 806 (2000).
[4] J. R. Abo-Shaeer, C. Raman, J. M. Vogels, and W. Ketterle, Science **292**, 476 (2001).
[5] S. Burger *et al.*, Phys. Rev. Lett. **83**, 5198 (1999).
[6] J. Denschlag *et al.*, Science **287**, 97 (2000).
[7] B. P. Anderson *et al.*, Phys. Rev. Lett. **86**, 2926 (2001).
[8] Z. Dutton, M. Budde, C. Slowe, and L. V. Hau, Science **293**, 663 (2001).
[9] B. B. Kadomtsev and V. I. Petviashvili, Sov. Phys. Dokl. **15**, 539 (1970); C. A. Jones, S. J. Putterman, and P. H. Roberts, J. Phys. A **19**, 2991 (1986); C. Josserand and Y. Pomeau, Europhys. Lett. **30**, 43 (1995); D. L. Feder *et al.*, Phys. Rev. A **62**, 053606 (2000); A. Muryshev *et al.*, Phys. Rev. Lett. **89**, 110401 (2002); G. Theocharis *et al.*, Phys. Rev. Lett. **90**, 120403 (2003).
[10] J. Brand and W. P. Reinhardt, J. Phys. B **34**, L113 (2001); J. Brand and W. P. Reinhardt, Phys. Rev. A **65**, 043612 (2002).
[11] S. Komineas and N. Papanicolaou, Phys. Rev. A **68**, 043617 (2003).
[12] N. G. Berloff, Phys. Rev. A **69**, 053601 (2004).
[13] L. V. Hau, S. E. Harris, Z. Dutton, and C. H. Behroozi, Nature (London) **397**, 594 (1999).
[14] L. V. Hau *et al.*, Phys. Rev. A **58**, R54 (1998).
[15] M. Andrews *et al.*, Science **275**, 637 (1997).
[16] C. J. Pethick and H. Smith, *Bose-Einstein Condensation in Dilute Gases* (Cambridge University Press, Cambridge, U.K., 2002).
[17] Y. Castin and R. Dum, Phys. Rev. Lett. **77**, 5315 (1996).
[18] Z. Dutton and L. V. Hau, Phys. Rev. A **70**, 053831 (2004).
[19] M. Machholm and H. Smith (private communication); L. D. Carr and C. W. Clark, cond-mat/0408460.